Chaos, Solitons and Fractals 116 (2018) 106–113

Contents lists available at ScienceDirect

Chaos, Solitons and Fractals

Nonlinear Science, and Nonequilibrium and Complex Phenomena

journal homepage: www.elsevier.com/locate/chaos

Frontiers

Effect of measuring noise on scaling characteristics in the dynamics of coupled chaotic systems

A.N. Pavlov[a,b,*], O.N. Pavlova[b], A.A. Koronovskii[b], A.E. Hramov[a]

[a] Yuri Gagarin State Technical University of Saratov, Politechnicheskaya Str. 77, Saratov 410054, Russia
[b] Saratov State University, Astrakhanskaya Str. 83, Saratov 410012, Russia

ARTICLE INFO

Article history:
Received 13 August 2018
Revised 12 September 2018
Accepted 17 September 2018

Keywords:
Scaling
Chaotic oscillations
Measuring noise
Return times
Correlation analysis

ABSTRACT

We study the scaling features in the evolutionary dynamics of two coupled chaotic systems based on the sequences of return times into a Poincaré section, contaminated with additive (measuring) noise. Using three models of chaotic systems: the Rössler oscillator, the Lorenz system, and the nephron model, and the detrended fluctuation analysis (DFA) as an approach for data processing, we demonstrate that the anti-correlated sequences of return times of synchronous motions show a higher sensitivity to measuring noise than the positively correlated series of return times of asynchronous oscillations. This conclusion is confirmed by the results for various oscillatory regimes in all models considered.

1. Introduction

A measured time series always contains noise of various origins [1]. Even if the dynamics of the system under study is deterministic, the conversion of the analog signal to digital format is accompanied by rounding errors, which can be treated as measuring noise. This type of noise does not influence the underlying dynamics of the system; however, it affects the accuracy of the evaluation of signal characteristics and the reliability of the diagnosis of the system's state from experimental data. A generally used approach to the processing of noisy data is its pre-filtering that can significantly reduce noise impact, especially when the frequency ranges of the signal reflecting the system's dynamics and additive fluctuations do not overlap. In practice, such approach is typically used to remove high-frequency variations of a signal providing its smoothing, or to eliminate slow changes in the mean value treated as a trend for nonstationary time series. Over the past decades, filtering capabilities have been improved by means of wavelet-based techniques being able to extract localized fluctuations that are not removed with Fourier-based approaches [2–5].

Filtering does not always improve the characterization of noisy data sets. This is the case, e.g., when considering point processes, where information about the system's dynamics is encoded by the times of stereotype events, and the data set represents a sequence of time intervals between successive events [6]. Such a sequence is often a noise-like process, where external fluctuations are difficult to detect and eliminate. In this regard, the effect of additive noise on the characterization of the system's dynamics from measured data should be known for various types of complex processes. From general assumptions, it could be expected that a small noise would provide insignificant changes in signal characteristics in comparison with fluctuations of higher intensity. Nevertheless, the effect of relatively weak fluctuations can differ between signals of distinct complexity and various dynamical regimes.

In this study, we consider how measuring noise affects the scaling features of complex processes in the dynamics of two coupled chaotic oscillators characterized by the sequences of return times into a Poincaré section. Such systems demonstrate various entrainment forms, which depend on the coupling strength and the individual dynamics of the oscillators. Unlike the frameworks of the classical theory of synchronization for periodic oscillations that is accompanied by a locking of their frequencies or phases, chaotic synchronization includes a wider range of entrainment phenomena represented by full synchronization [7,8], phase synchronization [9,10], lag synchronization [11], and generalized synchronization [12–14]. The related entrainment influences the dynamics of individual oscillators and changes the scaling features of the return time sequences. In particular, chaotic synchronization typically reduces the degree of multifractality in these sequences [15], which can be treated as a kind of ordering appeared due to the coupling between interacting units. Besides changes in the multifractality, synchronous and asynchronous oscillations are often quantified by

* Corresponding author at: Yuri Gagarin State Technical University of Saratov, Politechnicheskaya Str. 77, Saratov 410054, Russia.
E-mail address: pavlov.alexeyn@gmail.com (A.N. Pavlov).

https://doi.org/10.1016/j.chaos.2018.09.029
0960-0779/

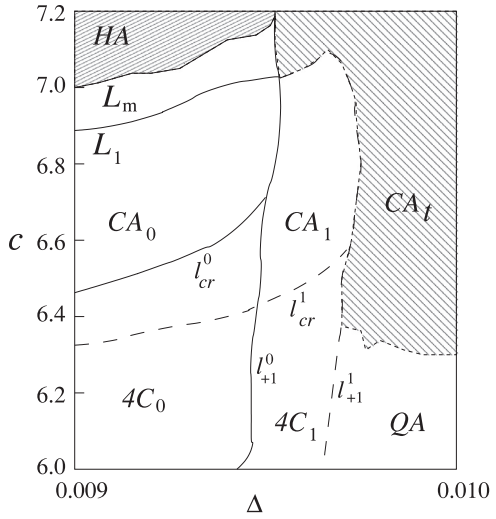

Fig. 1. A simplified bifurcation diagram of the model of two coupled Rössler oscillators.

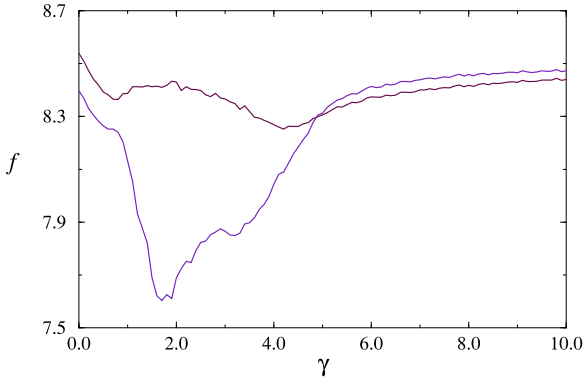

Fig. 2. Oscillation frequencies for two coupled Lorenz systems depending on the coupling strength.

different types of correlations, namely, by the anti-correlated sequences of return times related to synchronous dynamics and by positive correlations of return times for asynchronous regimes [15]. Distinctions in the structure of the return time sequences can exert different noise effect on the authentic characterization of the underlying dynamics from measured point processes.

Based on the detrended fluctuation analysis (DFA) [16–18], which is a widely used approach for studying the correlation properties of complex time series [19–24], we compare how measuring noise affects the error in characterizing the scaling features of various types of complex motions in the dynamics of interacting chaotic systems. We consider several models of chaotic oscillators including the Rössler system, the Lorenz oscillator and the nephron model, which exhibit oscillations with several different time scales, and show that the anti-correlated sequences of return times of synchronous motions demonstrate a higher sensitivity to measuring noise than the positively correlated series of return times of asynchronous oscillations. Such distinction in sensitivity to additive noise is confirmed for all models of coupled chaotic oscillators considered in this study.

2. Methods and models

2.1. Detrended fluctuation analysis

DFA is a variant of the correlation analysis of a data set, which is based on the transition to a random walk with its further root mean square analysis [16,17]. The algorithm includes the following four steps:

(1) The construction of a random walk $y(k)$ being a profile of the original data set $x(i)$, $i = 1, \ldots, N$:

$$y(k) = \sum_{i=1}^{k} [x(i) - \langle x \rangle], \tag{1}$$

where $\langle x \rangle$ is the mean value.

(2) Segmentation of $y(k)$ into non-overlapping parts of fixed size n and linear fitting inside each part to obtain a piecewise linear function $y_n(k)$ that describes a local trend.

(3) Computing the root mean-square fluctuation $F(n)$

$$F(n) = \sqrt{\frac{1}{N} \sum_{k=1}^{N} [y(k) - y_n(k)]^2}. \tag{2}$$

(4) Repeating the estimates for different n and computing the scaling exponent α, which describes the power-law behavior

$$F(n) \sim n^{\alpha}. \tag{3}$$

The value of α can be found as the slope of the dependence $F(n)$ in the log-log plot. This quantity relates to scaling exponents describing the behavior of the correlation function or the spectral power. For complex processes with a multiscale structure of data sets, $F(n)$ cannot be described by a simple power-law dependence with a single scaling exponent, and the local slopes of $\lg F$ vs. $\lg n$ vary depending on the size of the segment n. In this case, consideration of local scaling exponents seems preferable to a single quantity (global scaling exponent).

The values of $\alpha < 0.5$ quantify the anti-correlated statistics of the data samples $x(i)$, i.e. the alternation of large and small values of $x(i)$, when large values appear after small values and vice versa. Power-law correlations when large values mainly follow after large values and small values appear more often after small values are characterized by $\alpha > 0.5$. The uncorrelated dynamics of the data set is described by $\alpha = 0.5$.

2.2. Models of two coupled oscillators

2.2.1. Coupled Rössler systems

Two diffusively coupled Rössler oscillators represent a benchmark model of interacting nonlinear systems that produces a variety of complex dynamical regimes including regular, chaotic and hyperchaotic oscillations with different phase shifts between the signals of individual units. This model is described by six ordinary differential equations

$$\begin{aligned} \frac{dx_{1,2}}{dt} &= -\omega_{1,2} y_{1,2} - z_{1,2} + \gamma (x_{2,1} - x_{1,2}), \\ \frac{dy_{1,2}}{dt} &= \omega_{1,2} x_{1,2} + a y_{1,2}, \\ \frac{dz_{1,2}}{dt} &= b + z_{1,2}(x_{1,2} - c) \end{aligned} \tag{4}$$

The control parameters a, b and c define the dynamics of each system, and γ quantifies the coupling strength. The mismatch of the basic frequencies $\omega_1 = \omega_0 + \Delta$ and $\omega_2 = \omega_0 - \Delta$ provides non-identical oscillations of the interacting units. Here, we used the following parameter set: a=0.15, b=0.2, γ=0.02, ω_0=1 and varied the parameters c and Δ to analyze the transitions to and between different types of chaotic attractors or to a hyperchaotic regime. The phenomenon of phase multistability in the model (4) was discussed, e.g., in [25], where the bifurcation mechanisms leading to the appearance of various attractors are described. A simplified bifurcation diagram showing the main dynamical regimes discussed

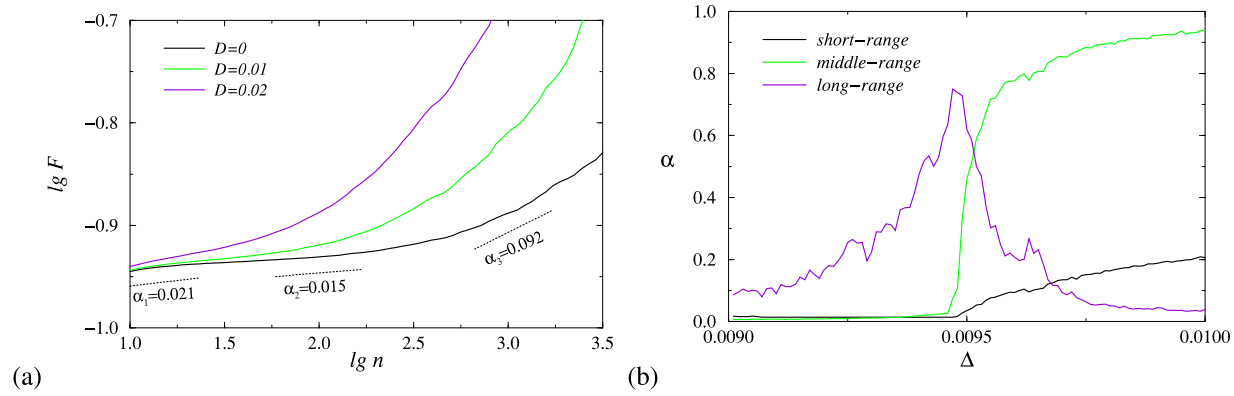

Fig. 3. The dependencies $F(n)$ in the lg-lg plot for different noise intensities (a), and the estimated scaling exponent α related to distinct ranges of the power-law correlations (b).

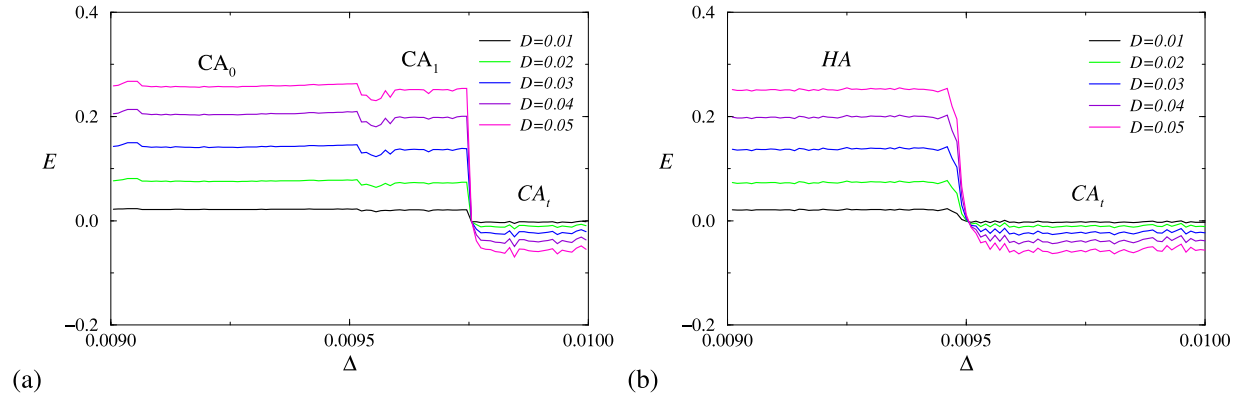

Fig. 4. Errors of estimation the α-value depending on the parameter Δ for c=6.8 (a) and c=7.2 (b) (the case of white noise).

in our study is given in Fig. 1. For more details, see the work by Postnov et al. [25].

Transition along the c-axis (for Δ near 0.009) realizes the period-doubling route to chaos with the appearance of the chaotic attractor CA_0. This synchronous regime is characterized by "in-phase" dynamics, i.e., by vanishing the phase difference of variables $x_1(t)$ and $x_2(t)$ for $\Delta = 0$. The chaotic attractor CA_1 also arises after the period-doubling cascade, however, it is characterized by a phase difference of 2π for the subharmonic components and relates to "out-of-phase" synchronous dynamics. Despite these regimes are quantified by distinct phase differences, their scaling features are nearly similar in comparison with asynchronous oscillations. With a further increase in c, the attractors CA_0 and CA_1 are merged leading to the hyperchaotic attractor HA. For Δ around 0.010, the range of c in Fig. 1 is related to asynchronous oscillations, namely, the quasiperiodic regime QA and the asynchronous chaotic attractor CA_t. An analysis of these regimes will be performed in Section 3 based on the sequences of return times into a Poincaré section that reflects the fractal structure of chaotic regimes. By analogy with the study [26], the secant plane $x_2 + y_1 = 0$ was selected.

2.2.2. Coupled Lorenz systems

Unlike the previous example (4), the coupled Lorenz systems demonstrate complex motions with clearly different time scales. This model is also described by six ordinary differential equations

$$\frac{dx_{1,2}}{dt} = \sigma(y_{1,2} - x_{1,2}) + \gamma(x_{2,1} - x_{1,2}),$$
$$\frac{dy_{1,2}}{dt} = r_{1,2}x_{1,2} - x_{1,2}z_{1,2} - y_{1,2},$$
$$\frac{dz_{1,2}}{dt} = x_{1,2}y_{1,2} - z_{1,2}b \quad (5)$$

with the parameters σ=10, r_1=28.8, r_2=28, and b=8/3 defining the oscillations of each unit and the coupling strength γ. Two types of motions are easily detected in the dynamics of individual oscillators. The first type is switching between the states "+1" ($x_{1,2} > 0$) and "−1" ($x_{1,2} < 0$), if each unit is treated as a bistable system [27]. The mean switching frequency depends on both, a parameter set characterizing the dynamical regime which occurs without coupling, and the strength of interaction. A relatively faster time scale characterizes the rotation (oscillation) of the phase space trajectory around unstable focus points. The peculiarity of the model (5) is a rather atypical behavior with increasing coupling strength [28]. Although the large values of the parameter γ provide the adjustment of the frequencies of both units (Fig. 2), the choice of the coupling strength in the range of $\gamma \in [0.0, 2.0]$ produces the opposite effect of the initial desynchronization. The analysis of the model (5) will be performed using the sequences of return times into the secant plane introduced as z_1=30.

2.2.3. Interacting nephrons

Two nephrons are another example of complex interacting oscillators possessing several different time scales. It describes the dynamics of the coupled functional units of the kidney which demonstrate the oscillations of tubular hydrostatic pressure and renal plasma flow. The autoregulation of blood flow at the level of single nephron can be simulated by six ordinary differential equations [29]:

$$\frac{dP_t}{dt} = G(P_t, r),$$

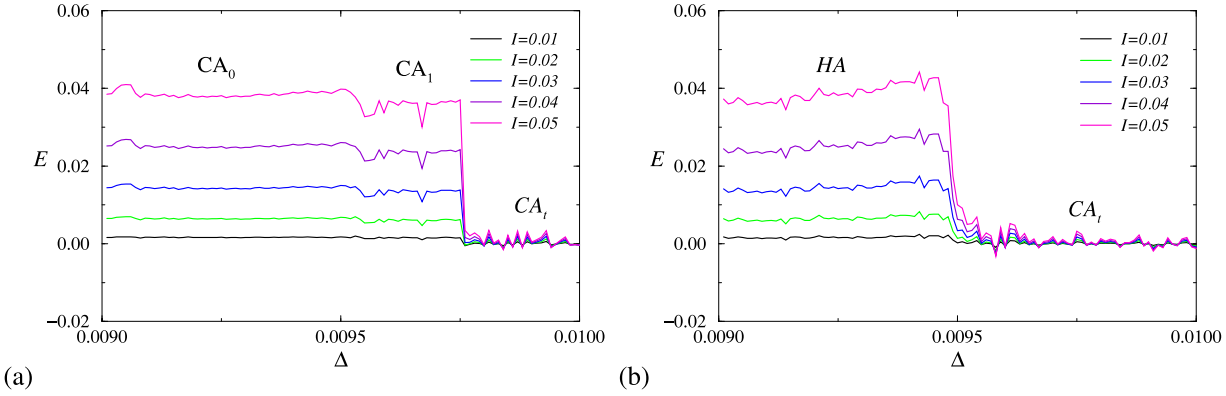

Fig. 5. Errors of estimation the α-value depending on the parameter Δ for c=6.8 (a) and c=7.2 (b) (the case of 1/f-noise).

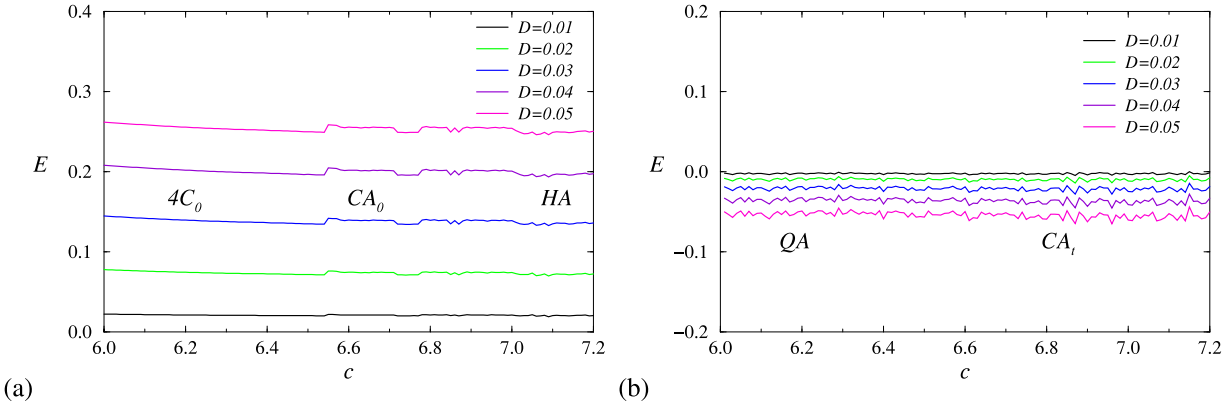

Fig. 6. Errors of estimation the α-value depending on the parameter c for Δ=0.009 (a) and Δ=0.010 (b).

$$\begin{aligned}
\frac{dr}{dt} &= v_r,\\
\frac{dv_r}{dt} &= V_{\beta,T}(P_t, r, \beta, X_3),\\
\frac{dX_1}{dt} &= \frac{3}{T}(F_H(P_t) - X_1),\\
\frac{dX_2}{dt} &= \frac{3}{T}(X_1 - X_2),\\
\frac{dX_3}{dt} &= \frac{3}{T}(X_2 - X_3).
\end{aligned} \tag{6}$$

Here, P_t is the proximal tubular pressure, G is a nonlinear function characterizing the filtration in *glomerulus*, r is the radius of the vessel, and v_r quantifies the rate of its variations. Equations for X_1, X_2 and X_3 introduce a delay T in the tubulo-glomerular feedback. The nonlinear function $V_{\beta,T}$ depends on X_3, which describes the positive feedback mechanism leading to the appearance of slow oscillations of P_t with the frequency of 0.02–0.04 Hz. The equations for r and v_r describe the myogenic mechanism that regulates renal blood flow and the glomerular filtration rate with the frequency of 0.1–0.2 Hz. Experiments [30,31] have established that the development of hypertension in rats is accompanied by a transition from nearly periodic oscillations of P_t to chaotic dynamics. An important parameter is the strength of the feedback regulation β, which increases in hypertensive rats. Because of the complex structure of nonlinear functions, we do not reproduce here the complete details of the nephron model (6) and its parameters that can be found in Ref. [29].

There are two mechanisms of interaction between neighboring nephrons, namely, the vascularly propagated interaction based on electrochemical signals (the main mechanism) and the hemodynamics interaction which has a weaker effect on the cooperative dynamics of coupled units of the kidney. We consider the first mechanism quantified by the coupling strength γ and introduce the secant planes P_t=1.6 kPa (to study the slow dynamics of the coupled nephrons) and v_r=0 (to consider the fast oscillations). A comparative analysis of noise effect will be performed for phase-locked chaotic dynamics ($T_1 = T_2$ =13.5 s, γ=0.005, β=27.3, where T_1 and T_2 denote the feedback delay for each of the coupled nephrons) and asynchronous chaos (T_1=13.5 s, T_2=13.4 s, γ=0.005, β=27.3). A detailed description of the interaction effects in coupling nephrons, including phase portraits and bifurcation diagrams, is given in Ref. [32].

3. Results and discussion

For all the models considered, we extracted the sequences of return times related to different values of control parameters and added a normally distributed random process (white noise) with the intensity D. Thus, we analyze the case of “measuring” noise that does not influence the dynamics of coupled oscillators (i.e., does not change the dynamical regime produced by the model in contrast to the case of fluctuations in model equations that can vary the control parameters) and only affects the quality of detection of distinct dynamical regimes.

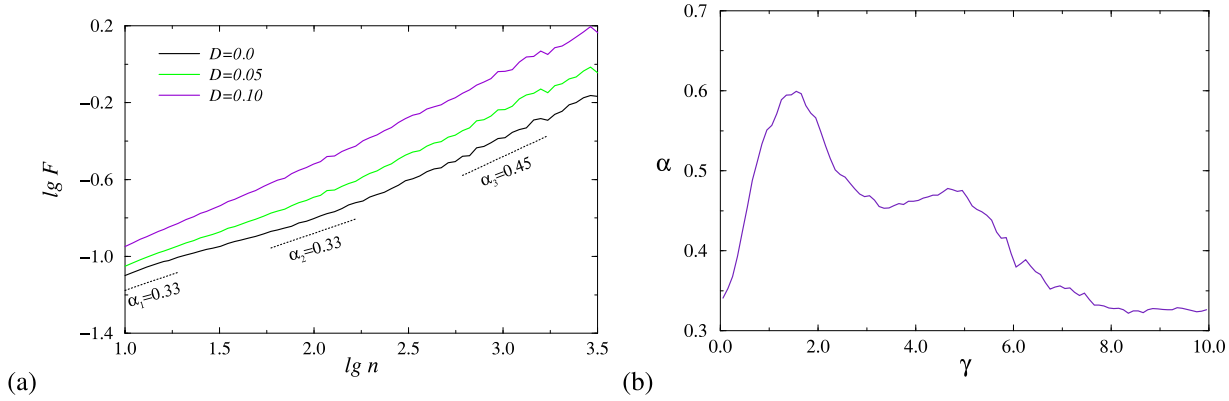

Fig. 7. The dependencies $F(n)$ in the lg-lg plot for different noise intensities (a), and the estimated scaling exponent α related to distinct ranges of the power-law correlations for D=0 (b).

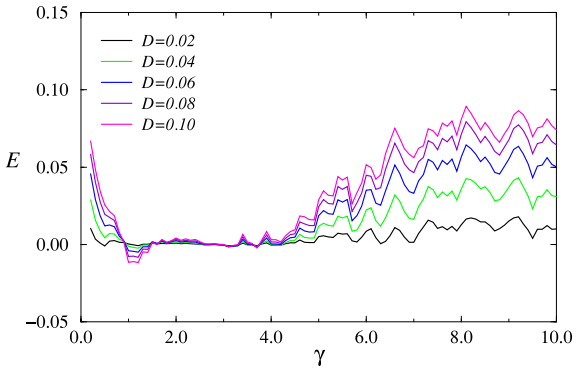

Fig. 8. Errors of estimation the α-value depending on the parameter γ for different noise intensities.

3.1. Coupled Rössler systems

Complex oscillations in the dynamics of two coupled Rössler systems are characterized by a multiscale structure, and the degree of multiscality varies between synchronous and asynchronous regimes [15]. Due to this, the scaling exponent α depends on the time scale. Fig. 3a illustrates the dependencies of $\lg F$ vs. $\lg n$ for the hyperchaotic attractor *HA* which was selected as the most complicated regime of the model (4). Unlike earlier study, here we discuss noise effect on the scaling features of complex oscillation and consider the cases of short-range correlations ($n \sim 10$), middle-range correlations ($n \sim 100$), and long-range correlations ($n \sim 1000$). According to Fig. 3a, the local slopes of the dependence $\lg F$ vs. $\lg n$ are different, although α-values are quite similar in the first two ranges for noiseless dynamics. The presence of noise in return times increases the scaling exponents, however, the related changes may differ between the ranges of scales. To illustrate this circumstance, variations of α-values with control parameters are considered. Fig. 3b shows the results for c=7.2 in the range $\Delta \in [0.009; 0.010]$ that includes the transition from the synchronous hyperchaotic attractor *HA* to the asynchronous chaotic regime CA_t around Δ=0.0095. Although this transition can be detected based on α-values when analyzing short-range correlations, a consideration of middle-range correlations provides a more informative characterization of the structural changes in the sequences of return times.

Let us now compare the effect of a measuring noise on characterization of these regimes from the return time sequences with added fluctuations of different intensity by estimating α as the local slope of the dependence (3) in the region around $n \sim 100$. Fig. 4a illustrates the results for noise intensities in the range [0.01; 0.05]. Since α-values of noiseless dynamics differ between the attractors *HA* and CA_t, a comparative analysis is performed for the absolute error

$$E = \alpha_{noi} - \alpha_0, \tag{7}$$

where α_0 is the value estimated for the noiseless dynamics of the coupled oscillators, and α_{noi} is the value obtained in the presence of additive fluctuations. According to Fig. 4a, measuring noise exerts about 5-fold stronger influence on the synchronous dynamics associated with the attractor *HA* than for the asynchronous chaotic dynamics CA_t. Therefore, the characterization of synchronous hyperchaotic oscillations from point processes contaminated with noise is a more complicated procedure.

In the example considered, we compared two oscillatory regimes of different complexity. Fig. 4b shows that a similar conclusion follows from an analysis of other types of interactive dynamics, namely, the synchronous chaotic oscillations CA_0 and CA_1 compared to the asynchronous chaos CA_t. Again, asynchronous oscillations are easier characterized from noisy return times since the presence of fluctuations provides significantly reduced variations in the scaling characteristics.

In an effort to study the effects of different types of noise, we considered colored noise instead of Gaussian noise. As a rule, the effects are very similar. Fig. 5 shows an example of the analysis performed for the case of $1/f$ noise with an intensity I. Here, the difference between synchronous and asynchronous dynamics is even better expressed compared to Fig. 4. Analogous results are obtained for other models where colored noise provides similar conclusions.

According to Fig. 6, noise effect is comparable when considering different types of synchronous or asynchronous dynamics. Thus, Fig. 6a illustrates nearly similar absolute errors of computing the scaling exponent α in a wide range of c-values (for Δ=0.009), which includes a period-doubling cascade and the merging of chaotic attractors leading to hyperchaos. Therefore, similar noise effect appears independently on the complexity of the dynamics. By analogy, the transition from the quasiperiodic oscillations (*QA*) to the chaotic regime (CA_t) is also characterized by similar α-variations (Fig. 6b). The differentiation between the scaling exponents of noiseless and noisy sequences of return times is much stronger between synchronous and asynchronous regimes, regardless of the type of underlying dynamics. We explain this circumstance by different correlation properties of point processes. Asynchronous dynamics is mainly associated with positive correlations of the return time sequences with $\alpha > 0.5$, whereas synchronous regimes are usually related to the anti-correlated structure of return times with $\alpha < 0.5$. Recent studies [33,34] discussed the effect

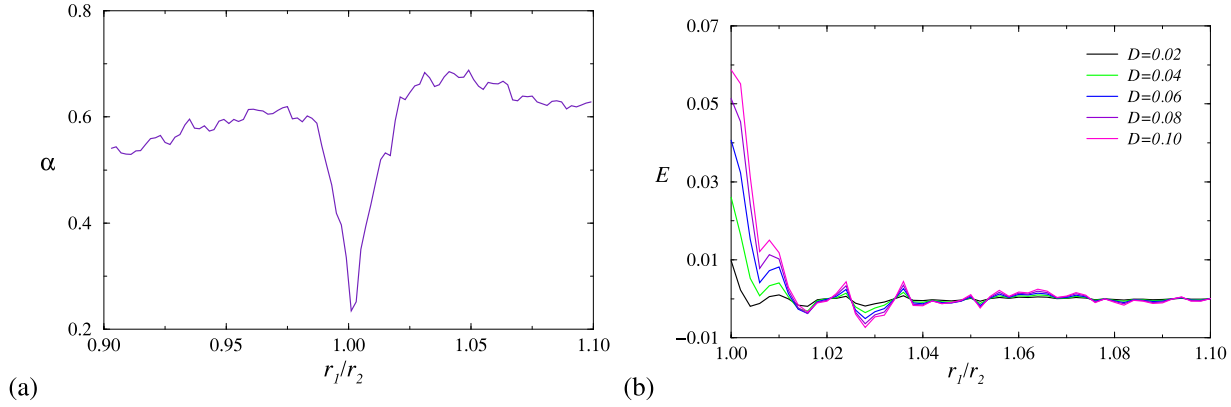

Fig. 9. The dependence of α from the ratio r_1/r_2 (a) and the estimated errors for different values of noise intensity (b).

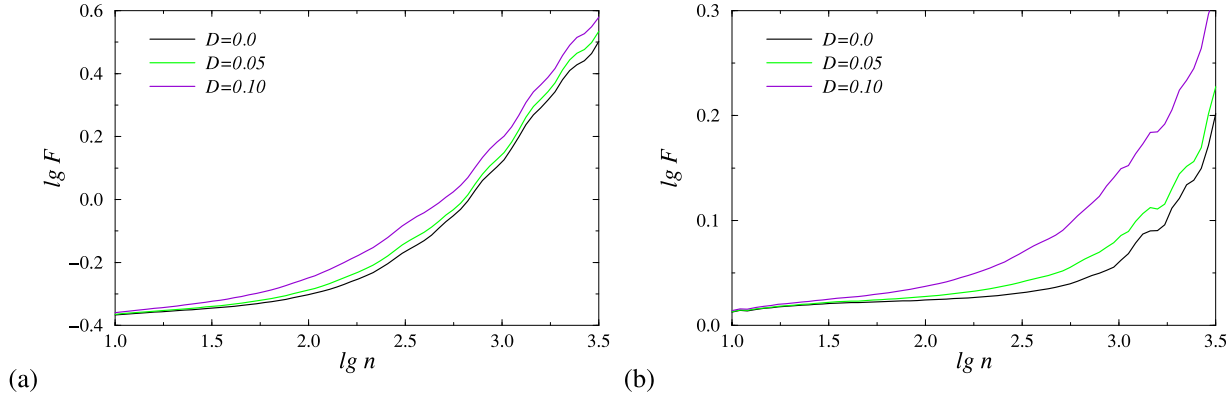

Fig. 10. The dependencies $F(n)$ in the lg-lg plot for slow (a) and fast (b) oscillations in the dynamics of coupled nephrons for distinct values of noise intensity.

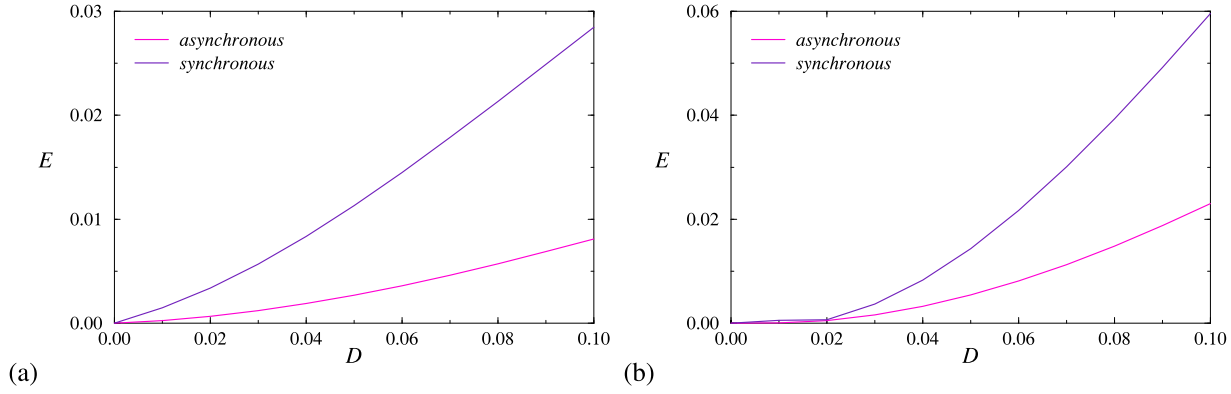

Fig. 11. Errors of estimation the scaling exponent α for synchronous and asynchronous motions in the dynamics of coupled nephrons related to slow (a) and fast (b) oscillatory modes depending on noise intensity.

of missing data on their scaling properties based on several examples of noise and showed that the absence of some data segments due to artifacts leads to stronger variations in scaling characteristics for anti-correlated dynamics. Although here we do not exclude some data fragments that provide a change in the correlation properties of the remaining data, the consideration of measuring noise can be interpreted as a partial loss of information about the deterministic dynamics of interacting oscillatory units. Therefore, the conclusions of [33,34] on the different sensitivity of anti-correlated and positively correlated data to missing information can be extended for the case of synchronous and asynchronous dynamics contaminated with noise.

3.2. Coupled Lorenz systems

The dynamics of the coupled Lorenz systems with the chosen set of parameters demonstrates smaller differences of α-values with varying time scale (Fig. 7a). Thus, the scaling properties of short- and middle-range correlations are nearly similar. The increase in α for long-range correlations is also much less pronounced compared to the previous model (Fig. 3a). Fig. 7b shows a typical dependence of α vs. the coupling strength γ. The initial desynchronization of oscillations with a maximum difference of frequencies around $\gamma = 1.5$ is accompanied by a correlated structure of return times with $\alpha \simeq 0.6$. With an increase in γ in the

range [1.5; 5.0], the scaling exponent reduces to $\alpha = 0.5$ (in this interval of γ, stochastic time scales are tuned, namely the switching frequencies). Further, for $\gamma > 5$, synchronization of oscillations occurs, and α reduces to 0.35 (γ=10), which indicates a transition to anti-correlated statistics of return times.

To illustrate the different sensitivity of return time sequences associated with synchronous and asynchronous dynamics of coupled units to measuring noise, we estimated the absolute error of computing α-values in the presence of additive fluctuations (7) – Fig. 8. According to this Figure, asynchronous dynamics ($\gamma \in [1.5; 5]$) is characterized by insignificant changes in α-values in comparison with the case of synchronization ($\gamma > 5$). This effect can be illustrated by changing the ratio of r-parameters of interacting systems with a fixed coupling strength. Fig. 9a shows a typical example of how the scaling exponent is varied with the ratio r_1/r_2. This Figure clearly illustrates the transition from correlated statistics of return times of asynchronous regimes ($\alpha > 0.5$) to anti-correlated statistics inside the synchronization "tongue" ($\alpha < 0.5$). Based on previous estimates, we expect that return time sequences inside the synchronization region are more sensitive to measuring noise. Fig. 9b confirms this assumption, showing that the strongest changes in α-values appear for identical systems ($r_1 = r_2$), and the added fluctuations do not significantly affect estimations of scaling exponents outside the synchronization region (e.g., the error E is close to zero for $r_1/r_2 = 1.1$). Thus, the results for interacting Lorenz systems confirm the conclusions for two coupled Rössler systems demonstrating the different sensitivity of synchronous oscillations (with anti-correlated statistics of return time sequences) and asynchronous oscillation (characterized by positive correlations of return times) to measuring noise in point processes analyzed in this study.

3.3. Interacting nephrons

In the dynamics of coupled Lorenz systems, two different time scales can be introduced: a stochastic time scale related to the switching frequency, and a deterministic time scale associated with the frequency of oscillations. The nephron model enables us to consider two deterministic time scales, namely, fast and slow dynamics. The interaction between neighboring nephrons leads to the interaction of these time scales, providing various regimes of full synchronization (when all time scales are adjusted), partial synchronization (adjustment of only one time scale in both units) and non-synchronous dynamics [35].

Analysis of the mathematical model (6) enables us to make a separation between fast and slow motions by introducing two secant planes and consideration the return times for slow and fast variables. Both these types of motions are characterized by nonlinear dependences $\lg F$ vs $\lg n$ that are illustrated in Fig. 10 for slow (Fig. 10a) and fast (Fig. 10b) oscillations. Estimating the scaling exponent α related to middle-range correlations, we performed a more detailed analysis of noise effect in detecting the scaling features of both types of motions. Fig. 11 shows how the absolute error depends on the intensity of fluctuations added to return times. For both slow and fast dynamics, measuring noise increases errors in detection scaling features of synchronous oscillations. This effect is observed for all noise intensities considered in our analysis (Fig. 11). Thus, the error ratio for synchronous and asynchronous oscillations is about 3.5 (D=0.1, slow motion) and about 2.7 (D=0.1, fast motion). Although the given distinctions are smaller in comparison, e.g., with the dynamics of the coupled Rössler systems, the general conclusion about stronger sensitivity of anti-correlated sequences of return times of synchronous motions to additive noise in comparison with positive correlated series of return times of asynchronous oscillations are confirmed for all examples of complex dynamics considered in this study.

4. Conclusion

Cooperative dynamics of interacting chaotic systems produce a variety of oscillatory regimes of different complexity. Characterization of these regimes from experimental data is influenced by additive fluctuations (measuring noise) that can lead to large computational errors in comparison with noiseless dynamics. Aiming to quantify the effect of noise on the ability of authentic characterization of complex oscillations from the measured data sets such as the sequences of return times into the Poincaré section, here we analyze different types of synchronous and asynchronous motions using the detrended fluctuation analysis.

Considering three models of oscillatory units, namely, the Rössler oscillator, the Lorenz system and the nephron model, and distinct types of regular and chaotic attractors, we showed essentially different effect of measuring noise on estimating the scaling features of synchronous and asynchronous dynamical regimes. These regimes are often quantified by different correlations in successive return times: the transition to the state of synchronous oscillations is accompanied by a reduced scaling exponent of the DFA-approach and a transition from positive correlations to anti-correlations in the return time series. The related distinctions can be a reason of a different effect of additive noise on the estimation of scaling exponents. Our analysis led to the conclusion that synchronous oscillations in the dynamics of coupled chaotic systems show a much stronger differentiation between the scaling exponents of noiseless and noisy sequences of return times than asynchronous oscillations. Therefore, the measured data sets of synchronous oscillatory regimes produce significantly higher errors of correlation analysis. This conclusion is confirmed for both, white or colored noise presented in the sequences of return times.

Acknowledgments

This work was supported by the Russian Science Foundation (Agreement 14-12-00224).

References

[1] Bendat JS, Piersol AG. Random data analysis and measurement procedures. 4th. New Jersey: Wiley; 2010.
[2] Kingsbury NG. Complex wavelets for shift invariant analysis and filtering of signals. J Appl Comput Harm Anal 2001;10:234.
[3] Selesnick IW, Baraniuk RG, Kingsbury NG. The dual-tree complex wavelet transform. IEEE Signal Process Mag 2005;22(6):123.
[4] Barri A, Dooms A, Schelkens P. The near shift-invariance of the dual-tree complex wavelet transform revisited. J Math Anal Appl 2012;389:1303.
[5] Sosnovtseva OV, et al. Interference microscopy under double-wavelet analysis: A new approach to studying cell dynamics. Phys Rev Lett 2005;94:218103.
[6] Daley DJ, Vere-Jones D. An introduction to the theory of point processes: volume I: Elementary theory and methods. Springer Science & Business Media; 2006.
[7] Pecora LM, Carroll TL. Synchronization in chaotic systems. Phys Rev Lett 1990;64:821.
[8] Fujisaka H, Yamada Y. Stability theory of synchronized motion in coupled-oscillator systems. Progr Theor Phys 1983;69:32.
[9] Rosenblum MG, Pikovsky AS, Kurths J. Phase synchronization of chaotic oscillators. Phys Rev Lett 1996;76:1804.
[10] Boccaletti S, et al. The synchronization of chaotic systems. Phys Rep 2002;366:1.
[11] Rosenblum MG, Pikovsky AS, Kurths J. From phase to lag synchronization in coupled chaotic oscillators. Phys Rev Lett 1997;78:4193.
[12] Rulkov NF, et al. Generalized synchronization of chaos in directionally coupled chaotic systems. Phys Rev E 1995;51:980.
[13] Kocarev L, Parlitz U. Generalized synchronization, predictability, and equivalence of unidirectionally coupled dynamical systems. Phys Rev Lett 1996;76:1816.
[14] Hramov AE, Koronovskii AA. An approach to chaotic synchronization. Chaos 2004;14(3):603.
[15] Pavlov AN, Sosnovtseva OV, Mosekilde E. Scaling features of multimode motions in coupled chaotic oscillators. Chaos Solitons Fractals 2003;16:801.
[16] Peng CK, et al. Mosaic organization of DNA nucleotides. Phys Rev E 1994;49:1685.
[17] Peng CK, et al. Quantification of scaling exponents and crossover phenomena in nonstationary heartbeat time series. Chaos 1995;5:82.

[18] Goldberger AL, et al. PhysioBank, PhysioToolkit, and PhysioNet: components of a new research resource for complex physiologic signals. Circulation 2000;101(23):e215.
[19] Talkner P, Weber RO. Power spectrum and detrended fluctuation analysis: Application to daily temperatures. Phys Rev E 2000;62:150.
[20] Hu K, et al. Effect of trends on detrended fluctuation analysis. Phys Rev E 2001;64:011114.
[21] Goldberger AL, et al. Fractal dynamics in physiology: alterations with disease and aging. PNAS 2002;99:2466.
[22] Bryce RM, Sprague KB. Revisiting detrended fluctuation analysis. Sci Rep 2012;2:315.
[23] Pavlov AN, et al. Detrended fluctuation analysis of EEG patterns associated with real and imaginary arm movements. Physica A 2018;509:777.
[24] Pavlova ON, et al. Effects of missing data on characterization of complex dynamics from time series. Commun Nonlinear Sci Numer Simulat 2019;66:31.
[25] Postnov DE, et al. Role of multistability in the transition to chaotic phase synchronization. Chaos 1999;9:227.
[26] Pavlov AN, et al. Characterization of the chaos-hyperchaos transition based on return times. Phys Rev E 2015;91:022921.
[27] Nicolis C, Nicolis G. Effective noise of the Lorenz attractor. Phys Rev A 1986;34:2384.
[28] Anishchenko VS, Silchenko AN, Khovanov IA. Synchronization of switching processes in coupled Lorenz systems. Phys Rev E 1988;57:316.
[29] Barfred M, Mosekilde E, Holstein-Rathlou NH. Bifurcation analysis of nephron pressure and flow regulation. Chaos 1996;6:280.
[30] Yip KP, Holstein-Rathlou NH, Marsh DJ. Chaos in blood flow control in genetic and renovascular hypertensive rats. Am J Physiol 1991;261:F400.
[31] Leyssac PP, Baumbach L. An oscillating intratubular pressure response to alterations in Henle loop flow in the rat kidney. Acta Physiol Scand 1993;117:415.
[32] Postnov DE, et al. Cooperative phase dynamics in coupled nephrons. Int J Mod Phys B 2001;15:3079.
[33] Ma QDY, et al. Effect of extreme data loss on long-range correlated and anticorrelated signals quantified by detrended fluctuation analysis. Phys Rev E 2010;81:031101.
[34] Pavlov AN, et al. Characterizing scaling properties of complex signals with missed data segments using the multifractal analysis. Chaos 2018;28:013124.
[35] Sosnovtseva OV, et al. Bimodal oscillations in nephron autoregulation. Phys Rev E 2002;66:061909.